

Phonon softening and “forbidden” mode observed by Raman scattering in $\text{Na}_{0.5}\text{CoO}_2$

Qingming Zhang,^{1,2,*} Ming An,² Shikui Yuan,² Yong Wu,² Dong Wu,³ Jianlin Luo,³ Nanlin Wang,³ Wei Bao,⁴ and Yening Wang²

¹*Department of Physics, Renmin University of China, Beijing 100872, P. R. China*

²*National Laboratory of Solid State Microstructures,*

Department of Physics, Nanjing University, Nanjing 210093, P. R. China

³*Beijing National Laboratory for Condensed Matter Physics, Institute of Physics, Chinese Academy of Sciences, Beijing 100080, P. R. China*

⁴*Los Alamos National Laboratory, Los Alamos, New Mexico 87545, USA*

(Dated: September 12, 2021)

Polarized Raman scattering measurements have been performed on $\text{Na}_{0.5}\text{CoO}_2$ single crystal from 8 to 305 K. Both the A_{1g} and E_{1g} phonon modes show a softening below $T_{c1} \approx 83$ K. Additionally, the A_{1g} phonon mode, which is forbidden in the scattering geometry of cross polarization for the triangular CoO_2 layers, appears below T_{c1} . In contrast, the metal-insulator transition at $T_{c2} \approx 46$ K has only secondary effect on the Raman spectra. The phonon softening and the “forbidden” Raman intensity follow closely magnetic order parameter and the gap function at the Fermi surface, indicating that the distortion of CoO_6 octahedra at T_{c1} , instead of the Na ordering at ~ 350 K, is the relevant structural component of the 83 K phase transition.

PACS numbers: 74.30.-j, 71.27.+a, 74.25.Kc

I. INTRODUCTION

The layered cobaltates Na_xCoO_2 are well known for their ionic mobility¹. Recently, their electronic properties have attracted much interest due to the discovery of superconductivity when water is intercalated². The Co ions form a triangular lattice in the CoO_2 planes, which are separated by Na^+ ions. With varying Na^+ content x , the valence of Co ions can be tuned from Co^{4+} (low spin $S = 1/2$) to Co^{3+} ($S = 0$). Analogy to the high transition-temperature cuprate superconductors has been drawn, since Na_xCoO_2 may be regarded as doping a $S = 1/2$ Mott insulator on a triangular lattice². However, the Na^+ layers serve not only as charge reservoirs. Order of Na^+ ions at specific concentrations dramatically affect electronic properties, such as the insulating state at $x=0.5$ sandwiched by metallic states at lower and higher dopings^{3,4}. Additionally, the valence of Co ions in the hydrated superconductor $\text{Na}_{0.35}\text{CoO}_2 \cdot 1.3\text{H}_2\text{O}$ is suggested in recent studies to be close to +3.5 rather than the apparent +3.7, caused by the isovalent exchange of the hydronium ion H_3O^+ and $\text{Na}^{+5,6}$. Hence, Na_xCoO_2 with $x=0.5$ instead of $x \sim 0$ may be regarded as the parent compound of the hydrated superconductor. Therefore, it is of particular interest to focus on $\text{Na}_{0.5}\text{CoO}_2$.

A metal-insulator transition (MIT) at $T_{c2} \sim 51$ K is clearly indicated in transport and infrared measurements of $\text{Na}_{0.5}\text{CoO}_2$ ^{3,7}. The transition is marked also by a depression in magnetic susceptibility. In addition, another anomaly in magnetic susceptibility occurs at $T_{c1} \sim 88$ K, where the spins form an alternating antiferromagnetic pattern in the CoO_2 plane^{8,9} and the Hall coefficient abruptly changes sign³. The MIT has been explained as a consequence of charge ordering³, and structure data from electron and neutron diffraction measurements have been explained by alternating $\text{Co}^{3.5+\delta}$ and $\text{Co}^{3.5-\delta}$ chains, dec-

orated by an ordered Na^+ pattern which exists already at the room temperature^{4,10}. However, the charge segregation into $\text{Co}^{3.5\pm\delta}$ is disputed by a recent NMR study, and an alternative explanation of nesting of the Fermi surface at the lower orthorhombic symmetry is provided¹¹. The nesting of the Fermi surface is also used to explain the angle-resolved photoemission spectroscopy (ARPES) experiments¹². The subtle relation between electronic, magnetic and structural properties also manifests in the restoration of the triangular symmetry of $\text{Na}_{0.5}\text{CoO}_2$ at high magnetic fields¹³.

Although a link between Na^+ ordering, which breaks the triangular symmetry, and the phase-transitions at T_{c1} and T_{c2} in $\text{Na}_{0.5}\text{CoO}_2$ has been suggested through Co charge segregation, the relation between structure and the successive transitions can not be unambiguously determined in the crystallography studies due to the limited sensitivity of the diffraction techniques^{4,10}. In addition, no anomaly in lattice dynamics has been reported at these transitions in $\text{Na}_{0.5}\text{CoO}_2$. Here we present polarized Raman scattering measurements on single crystalline sample of $\text{Na}_{0.5}\text{CoO}_2$ from 8 to 305 K. Phonon softening is observed below T_{c1} for both the A_{1g} and E_{1g} modes of the CoO_6 octahedra. Simultaneously, the forbidden A_{1g} mode in the channel of cross polarization appears at T_{c1} . It indicates that the transition at T_{c1} is not only magnetic or electronic, but also involved with structural distortion of the CoO_6 octahedra. The distortion in the CoO_2 plane, instead of the orthorhombic Na ordering at ~ 350 K^{3,4}, is more directly related to the phase transition probed in the NMR, ARPES and neutron diffraction experiments at T_{c1} .

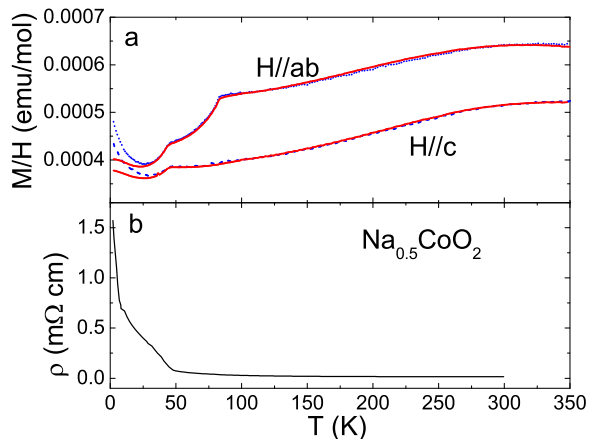


FIG. 1: (color online) Temperature dependence of (a) magnetic susceptibility and (b) in-plane resistivity of $\text{Na}_{0.5}\text{CoO}_2$. The blue dashed and red solid curves in (a) were measured in a magnetic field of 1 and 12 T, respectively.

II. EXPERIMENTAL DETAILS

Single crystal samples of Na_xCoO_2 were grown using a traveling solvent floating-zone furnace. The as-grown crystal was cut into pieces with the dimensions of $\sim 2 \times 2 \times 0.2 \text{ mm}^3$ and has a starting sodium concentration of about 0.75. After the chemical deintercalation of Na in solutions of I_2 dissolved acetonitrile, the actual Na concentration was determined to be $x=0.5 \pm 1\%$ by inductively coupled plasma spectrometry. The detailed procedure for preparing high-quality single crystal samples can be found elsewhere¹⁴. The susceptibility and resistivity of the $\text{Na}_{0.5}\text{CoO}_2$ single crystal used in the Raman study are shown in Fig. 1. They are in good agreement with published results^{3,7,8,9,10,11,12}, with $T_{c2} \approx 46 \text{ K}$ and $T_{c1} \approx 83 \text{ K}$.

The Raman measurements were performed with a double-gratings monochromator (Jobin Yvon U1000). The detector is a back-illuminated CCD cooled by liquid nitrogen. An argon ion laser was used with an excitation wavelength of 514.5 nm. The laser beam of 3 mW was focused into a spot of ~ 70 microns in the diameter on the sample surface. The temperature increase by laser heating is less than 10 K and was calibrated in the measurements. The sample was mounted in a liquid helium cryostat with a vacuum of $\sim 10^{-7}$ torr. The data was collected with a pseudo-backscattering configuration. Perfect surface was obtained after cleavage, and the crystal orientation was determined by the Laue pattern before the sample was mounted in the cryostat.

III. RESULTS AND DISCUSSIONS

The edge-shared CoO_6 octahedra in Na_xCoO_2 form triangular planes¹⁰. The polarization of light along the Co-O bond orientation is denoted as x, and the perpen-

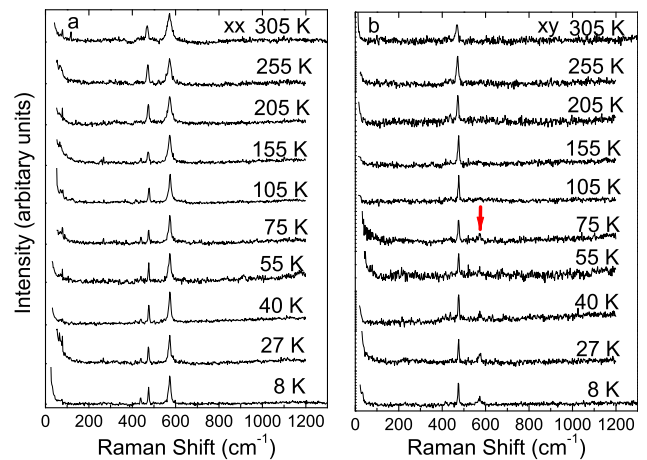


FIG. 2: (color online) Polarized Raman spectra at various temperatures. (a) In the xx channel, both E_{1g} and A_{1g} modes are allowed. (b) In the xy channel, only the E_{1g} mode is active. However, the “forbidden” A_{1g} mode near 573 cm^{-1} grows in the xy channel below $T_{c1} \approx 83 \text{ K}$, as indicated by the arrow.

dicular orientation in the CoO_2 plane as y. A standard calculation of the Raman tensors shows that the in-plane E_{1g} mode of oxygen vibrations in the CoO_6 octahedra is allowed in both the xx and xy channels. The out-of-plane A_{1g} mode, however, is allowed only in the xx channel. Polarized Raman spectra in the xx and xy channels, measured at various temperatures, are shown in Fig. 2. The wavenumbers of the E_{1g} and A_{1g} modes are 469 cm^{-1} and 572 cm^{-1} , respectively, at 305 K. They are consistent with published data on Na_xCoO_2 and $\text{Na}_x\text{CoO}_2 \cdot y\text{H}_2\text{O}$ ^{15,16,17} and first-principles calculations^{18,19}.

The wavenumbers of the E_{1g} and A_{1g} modes are shown in Fig. 3 as a function of temperature. As the sample was cooled from the room temperature to T_{c1} , the phonon wavenumbers of both modes increase gradually. The increase can be understood naturally in terms of anharmonic effect which has also been reported previously¹⁶. It includes two contributions: one from thermal expansion and the other from multi-phonon decay process^{20,21}. The contribution from thermal expansion can be written as $-3\omega_0\gamma \cdot \Delta a/a$, where ω_0 is the zero-temperature phonon frequency, γ the Grüneisen constant, and $\Delta a/a$ the linear thermal expansion^{22,23}. Neutron diffraction shows that the average in-plane $\Delta a/a$ is 16 ppm, whereas $\Delta a/a$ is 2540 ppm for the c-axis²⁴. Since the E_{1g} (A_{1g}) phonon mode is related to the in-plane (out-of-plane) vibrations of oxygen atoms in the CoO_6 octahedra, the wavenumbers should be sensitive to the change of the in-plane bonds rather than the c-axis expansion. Hence, the small in-plane $\Delta a/a$ would translate to a small anharmonic contribution from thermal expansion.

The main contribution to the shift of phonon wavenumbers above T_{c1} then can be reasonably attributed to multi-phonon decay process. For a three-

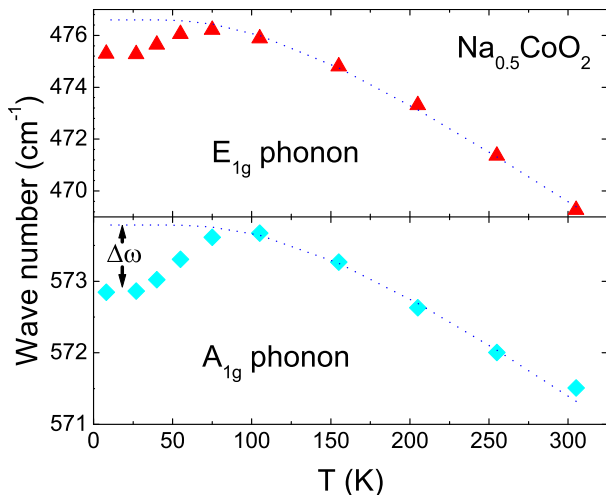


FIG. 3: (color online) Temperature dependence of the E_{1g} and A_{1g} phonon wavenumbers. The dotted curves are the least-square fitting of data taken above 83 K to Eq. (1) for anharmonic effect, and phonon softening $\Delta\omega$ occurs below T_{c1} .

phonon process, a Raman optical phonon with the frequency of ω_0 will decay into two phonons with ω_1 and ω_2 , respectively, where $\omega_0 = \omega_1 + \omega_2$. The frequency shift by the process is

$$\omega - \omega_0 = -\alpha \cdot \left(\frac{1}{e^{\omega_1/kT} - 1} + \frac{1}{e^{\omega_2/kT} - 1} \right), \quad (1)$$

where α is a material-dependent constant^{20,25}. Klemens has considered the decay channels through acoustic phonons which fulfill the condition $\omega_1 = \omega_2$ ²¹. In many cases, it offers a good approximation. The dotted curves in Fig. 3 are the results of fitting data above T_{c1} to Eq. (1) under the Klemens condition with $\alpha = 7.5$ and 3.5 cm^{-1} for the E_{1g} and A_{1g} modes, respectively. The Klemens model describes well our data above T_{c1} , and the values of α are comparable with 13 cm^{-1} deduced from diamond, and 2 to 4 cm^{-1} for semiconducting materials such as AlN, Si, and GaAs^{25,26}.

When the sample was cooled further, the first new discovery of this work is that both the E_{1g} and A_{1g} modes soften considerably below the T_{c1} , departing from the dotted curves from the anharmonic effect (Fig. 3). The softening in frequency, $\Delta\omega$, is taken as the difference between the dotted curve and measured data. It is scaled so that it has the same value at 8 K for both the E_{1g} and A_{1g} modes, and it follows the same function of temperature for both modes as shown in Fig. 4.

Since an antiferromagnetic transition occurs at T_{c1} , it is natural to consider the spin-phonon coupling. In a magnetic material mediated by the superexchange interaction J , such as in magnetic insulators, the J would be

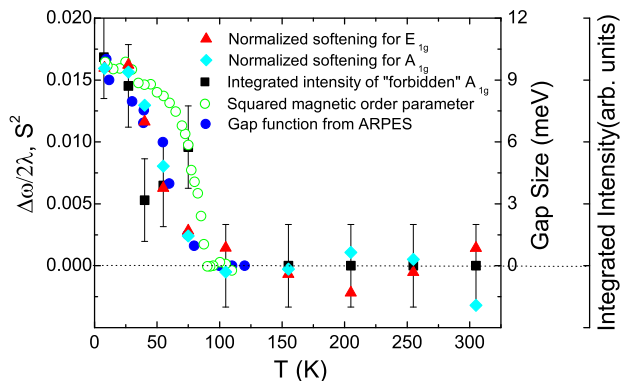


FIG. 4: (color online) Temperature dependence of phonon softening $\Delta\omega$ for the E_{1g} (red triangles) and A_{1g} (cyan diamonds) modes, and the integrated intensity of the “forbidden” A_{1g} mode in the xy channel (black squares). For details on λ , see text. The open green circles represent the squared magnetic order parameter S^{29} , and the filled blue circles the gap function at the Fermi surface¹².

modulated by the vibrating positions of ligands:

$$J(\mathbf{r}) = J(\mathbf{r}_0) + \left. \frac{\partial J}{\partial \mathbf{r}} \right|_{\mathbf{r}_0} \cdot (\mathbf{r} - \mathbf{r}_0) + \left. \frac{\partial^2 J}{\partial \mathbf{r}^2} \right|_{\mathbf{r}_0} (\mathbf{r} - \mathbf{r}_0)^2 + \dots, \quad (2)$$

where \mathbf{r} and \mathbf{r}_0 are the instantaneous and equilibrium positions of oxygen, respectively, in our case. Usually spin-phonon coupling is a second-order effect since the linear contribution is canceled out by the symmetric oscillation of ions around equilibrium positions. However, some local asymmetric structures would cause the linear part to be finite, such as the buckled CuO_2 plane in $\text{YBa}_2\text{Cu}_3\text{O}_{7-\delta}$ ²⁷. Similarly, in Na_xCoO_2 , the oxygen and cobalt ions are not in the same plane. The oscillation of oxygen ions is expected to have a strong effect on magnetic interaction J . The phonon softening due to the spin-phonon coupling can be expressed as^{28,29}

$$\Delta\omega = -\lambda \langle \mathbf{S}_i \cdot \mathbf{S}_{i+1} \rangle = 2\lambda S^2, \quad (3)$$

where λ is the spin-phonon coupling coefficient, $\langle \mathbf{S}_i \cdot \mathbf{S}_{i+1} \rangle$ the average for adjacent spin pairs, and $S^2 = (M/2g\mu_B)^2$ the squared magnetic order parameter. In evaluating $\langle \mathbf{S}_i \cdot \mathbf{S}_{i+1} \rangle$ in the last step of Eq. (3), neutron diffraction result by Gásparović et al.⁹ was used. In Fig. 4, measured S^2 for $\text{Na}_{0.5}\text{CoO}_2$ (open green circles)⁹ is compared with the scaled phonon softening for the E_{1g} (red triangles) and A_{1g} (cyan diamonds) modes. While both $\Delta\omega$ and S^2 appear below T_{c1} , the softening is slower and less mean-field-like than the squared magnetic order parameter, namely, the Eq. (3) is not perfectly followed. It is not clear whether this is due to $\text{Na}_{0.5}\text{CoO}_2$ not being an insulator above the 46 K metal-insulator transition. If one nevertheless applies Eq. (3) to $\text{Na}_{0.5}\text{CoO}_2$ at 8 K, which is then an insulator, the spin-phonon coupling coefficient λ is estimated as 30 cm^{-1} for the A_{1g} mode and 41 cm^{-1} for the E_{1g} mode, respectively. For comparison, λ is -50 cm^{-1} in CuO ²⁹, 6 and 9 cm^{-1} for two

phonon modes in $\text{Y}_2\text{Ru}_2\text{O}_7$ ³⁰, and $|\lambda|$ is less than 3 cm^{-1} for antiferromagnets in the rutile structure such as FeF_2 , MnF_2 and NiF_2 ²⁸. Thus, the spin-phonon coupling in $\text{Na}_{0.5}\text{CoO}_2$ is very strong.

The spin-phonon coupling is a *dynamical* spin-lattice interaction. At a magnetic transition, *static* spin-lattice interaction is also possible, which is usually referred to as magnetoelastic effect. The effect requires no phonon softening, but a static change of local structure. In addition to the phonon softening, the second new discovery of this work is that the A_{1g} mode in the “forbidden” xy channel also appears below T_{c1} in $\text{Na}_{0.5}\text{CoO}_2$, see Fig. 2(b). The violation of the Raman selection rules mentioned above for the triangular layers requires a structural distortion in the edge-shared CoO_6 to break lattice symmetry of the high temperature phase. Qualitatively, the integrated intensity of the “forbidden” A_{1g} mode is proportional to the distortion at low temperatures. In Fig. 4, the integrated intensity of the “forbidden” mode is plotted as the black squares. It follows the general trend of $\Delta\omega$, except that there appears a dip around T_{c2} . However, more sensitive experiments are called for to establish the statistical significance of the dip. Magnon scattering was suggested as the origin of the “forbidden” A_{1g} mode in view that the mode appears only below the magnetic transition. However, this explanation has difficulty for the same mode in the allowed xx channel at all measured temperatures.

In Fig. 4, the single-particle gap function (filled blue circles) from the ARPES measurements¹² is also plotted. Different from magnetic order parameter, it traces the phonon softening $\Delta\omega$ very well. On the other hand, the metal-insulator transition at T_{c2} has no detectable effect on either $\Delta\omega$ or the gap function. Although the gap is opened only at the a_{1g} Fermi surface of the Co ions, the Na ordering at $\sim 350 \text{ K}$ was invoked to provide a nesting condition for the Fermi surface¹². But Qian *et al.* also noticed that their observed gap is less anisotropic than expected from such a nesting scenario and that the gap size is rather soft compared to many CDW systems. In addition, the Fermi surface geometry does not share the two-fold symmetry of the Na supercell¹². Thus, our observed structural transition directly involving CoO_6 at the same temperature offers a promising alternative mechanism for the band folding. Similarly, the supercell

needed for explanation of the NMR results at T_{c1} ¹¹ may come instead from the distortion of the CoO_6 octahedra. We notice that electron diffraction experiments at 100 K detected from the Na layers another tripled superlattice pattern which, however, disappears at 20 K ^{4,10}. Whether the tripled superlattice pattern has anything to do with our observed CoO_6 distortion, which persists down to our lowest measurement temperature at 8 K , is not obvious.

IV. CONCLUSIONS

In summary, our polarized Raman measurements of $\text{Na}_{0.5}\text{CoO}_2$ single crystal have shed new light on the multiple phase transitions in the interesting material. Above $T_{c1} \approx 83 \text{ K}$, only conventional anharmonic effect was observed. The softening of the A_{1g} and E_{1g} optical phonon modes was observed below T_{c1} , accompanied by the A_{1g} mode in the “forbidden” xy Raman channel. Our results indicate a structural transition at T_{c1} which breaks the local lattice symmetry of the CoO_6 octahedra. The spin-phonon coupling in $\text{Na}_{0.5}\text{CoO}_2$ is among the strongest of magnetic materials. The closely related order-parameters of the structural distortion and phonon softening in the CoO_6 layers as well as the magnetic and electronic transitions involving electrons of Co ions suggests a common origin for these transitions. The structural condition for the nesting Fermi surface scenario which was invoked as the mechanism for the magnetic transition and the partial gapping of the Fermi surface at T_{c1} is more likely the structural distortion discovered in this work in the Co layers than the orthorhombic Na ordering at $\sim 350 \text{ K}$. If $\text{Na}_{0.5}\text{CoO}_2$ is indeed more appropriate as the parent compound of the superconducting $\text{Na}_{0.35}\text{CoO}_2 \cdot 1.3\text{H}_2\text{O}$ ^{5,6}, it may be difficult to exclude a lattice contribution to focus on a purely electronic superconducting mechanism.

V. ACKNOWLEDGMENTS

The authors would like to thank B. Normand, T. Li, Q. H. Wang, Z.-Q. Wang and Y. Chen for helpful discussions. The work was supported by the MOST of China (973 project No:2006CB601002) and NSFC Grant No. 10574064; WB was supported by the US DOE.

* Electronic address: qmzhang@ruc.edu.cn

¹ J. Molenda, C. Delmas, and P. Hagenmuller, *Solid State Ionics* **10**, 431 (1983); A. Stoklosa, J. Molenda, D. Than, *Solid State Ionics* **15**, 211 (1985); M. G. S. R. Thomas, P. G. Bruce, and J. B. Goodenough, *Solid State Ionics* **17**, 13 (1985).

² K. Takada, H. Sakurai, E. Takayama-Muromachi, F. Izumi, R. A. Dilanian, and T. Sasaki, *Nature (London)* **422**, 53 (2003).

³ M. L. Foo, Y. Y. Wang, S. Watauchi, H. Zandbergen, T.

He, R. J. Cava, and N. P. Ong, *Phys. Rev. Lett.* **92**, 247001 (2004).

⁴ H. W. Zandbergen, M. Foo, Q. Xu, V. Kumar, and R. J. Cava, *Phys. Rev. B* **70**, 024101 (2004).

⁵ P. W. Barnes, M. Avdeev, J. D. Jorgensen, D. G. Hinks, H. Claus, and S. Short, *Phys. Rev. B* **72**, 134515 (2005).

⁶ H. Sakurai, K. Takada, T. Sasaki, and E. Takayama-Muromachi, *J. Phys. Soc. Jpn* **74**, 2909 (2005).

⁷ N. L. Wang, D. Wu, G. Li, X. H. Chen, C. H. Wang, and X. G. Luo, *Phys. Rev. Lett.* **93**, 147403 (2004).

- ⁸ M. Yokoi, T. Moyoshi, Y. Kobayashi, M. Soda, Y. Yasui, M. Sato and K. Kakurai, *J. Phys. Soc. Jpn* **74**, 3046 (2005).
- ⁹ G. Gäsparović, R. A. Ott, J.-H. Hoo, F. C. Chou, Y. Chu, J. W. Lynn, and Y. S. Lee, *Phys. Rev. Lett.* **96**, 046403 (2006).
- ¹⁰ Q. Huang, M. Foo, J. Lynn, H. Zandbergen, G. Lawes, Y. Wang, B. H. Toby, A. Ramirez, N. Ong, and R. Cava, *J. Phys.: Cond. Matter* **16**, 5803 (2004).
- ¹¹ J. Bobroff, G. Lang, H. Alloul, N. Blanchard, and G. Collin, *Phys. Rev. Lett.* **96**, 107201 (2006).
- ¹² D. Qian, L. Wray, D. Hsieh, D. Wu, J. L. Luo, N. L. Wang, A. Fedorov, A. Kuprin, R. J. Cava, L. Viciu, and M. Z. Hasan, *Phys. Rev. Lett* **96**, 046407 (2006).
- ¹³ L. Balicas, M. Abdel-Jawad, N. E. Hussey, F. C. Chou, and P. A. Lee, *Phys. Rev. Lett.* **94**, 236402 (2005).
- ¹⁴ D. Wu, J. L. Luo, and N. L. Wang, *Phys. Rev. B* **73**, 014523 (2006).
- ¹⁵ M. N. Iliev, A. P. Litvinchuk, R. L. Meng, Y. Y. Sun, J. Cmaidalka, and C. W. Chu, *Physica C* **402**, 239 (2004).
- ¹⁶ P. Lemmens, K. Y. Choi, V. Gnezdilov, E. Ya. Sherman, D. P. Chen, C. T. Lin, F. C. Chou, and B. Keimer, *Phys. Rev. Lett.* **96**, 167204 (2006).
- ¹⁷ J. F. Qu, W. Wang, Y. Chen, G. Li, and X. G. Li, *Phys. Rev. B* **73**, 092518 (2006).
- ¹⁸ P. Zhang, W. Luo, V. H. Crespi, M. L. Cohen, and S. G. Louie, *Phys. Rev. B* **70**, 085108 (2004).
- ¹⁹ Z. Li, J. Yang, J. G. Hou, and Q. Zhu, *Phys. Rev. B* **70**, 144518 (2004).
- ²⁰ R. A. Cowley, *J. Phys. (Paris)* **26**, 659 (1965).
- ²¹ P. G. Klemens, *Phys. Rev.* **148**, 845 (1966).
- ²² J. Menendez and M. Cardona, *Phys. Rev. B* **29**, 2051 (1984).
- ²³ G. Lang, K. Karch, M. Schmitt, P. Pavone, A. P. Mayer, R. K. Wehner, and D. Strauch, *Phys. Rev. B* **59**, 6182 (1999).
- ²⁴ A. J. Williams, J. P. Attfield, M. L. Foo, L. Viciu, and R. J. Cava, *Phys. Rev. B* **73**, 134401 (2006).
- ²⁵ M. S. Liu, L. A. Bursill, S. Prawer, and R. Beserman, *Phys. Rev. B* **61**, 3391 (2000).
- ²⁶ D. Y. Song, M. Holtz, A. Chandolu, S. A. Nikishin, E. N. Mokhov, Yu. Makarov, and H. Helava, *Appl. Phys. Lett.* **89**, 021901 (2006); M. Balkanski, R. F. Wallis, and E. Haro, *Phys. Rev. B* **28**, 1928 (1983); C. Ramkumar, K. P. Jain, and S. C. Abbi, *Phys. Rev. B* **53**, 13672 (1996).
- ²⁷ B. Normand, H. Kohnno, and H. Fukuyama, *Phys. Rev. B* **53**, 856 (1996).
- ²⁸ D. J. Lockwood and M. G. Cottam, *J. Appl. Phys.* **64**(10), 5876 (1988); D. J. Lockwood, *Low Temp. Phys.* **28**, 505 (2002).
- ²⁹ X. K. Chen, J. C. Irwin, and J. P. Franck, *Phys. Rev. B* **52**, R13130 (1995).
- ³⁰ J. S. Lee, T. W. Noh, J. S. Bae, In-Sang Yang, T. Takeda, R. Kanno, *Phys. Rev. B* **69**, 214428 (2004).